

RECLAMATION

Managing Water in the West

PAP-1044

Noise Generation by Air Bubbles in Water: An Experimental Study of Creation and Splitting

**A Thesis Submitted to the Faculty
of the Graduate School of the
University of Minnesota**

By K. Warren Frizell

December 1987



U.S. Department of the Interior
Bureau of Reclamation
Technical Service Center
Hydraulic Investigations and Laboratory Services Group
Denver, Colorado

**Noise Generation by Air Bubbles in Water:
An Experimental Study of Creation and Splitting**

A THESIS

SUBMITTED TO THE FACULTY OF THE GRADUATE SCHOOL
OF THE UNIVERSITY OF MINNESOTA

BY

Kenneth Warren Frizell

IN PARTIAL FULFILLMENT OF THE REQUIREMENTS
FOR THE DEGREE OF
MASTER OF SCIENCE

December 1987

ABSTRACT

The study of two-phase flow, especially air-water mixtures, has received much attention over the years. Little has been done concerning the noise generated by non-cavitating air-water flows. The main purpose of this work is to examine these flows; in particular, to look at the noise associated with the creation of air bubbles at a nozzle, and the noise radiated by air bubbles splitting in the shear layer of a submerged turbulent water jet. Experiments were conducted to measure the sound pressure levels associated with bubble creation and bubble splitting, under a variety of conditions. Comparisons were made with existing theories. An improved physical understanding of the mechanism of noise generation was gained through data analysis and photographic studies. Recommendations for further research are given.

ACKNOWLEDGEMENTS

I am most grateful to Dr. Roger E. A. Arndt for his thoughtful guidance in the completion of this work. I have enjoyed the opportunity to work with him and I have learned much from his experience and approach to research. I would like to thank Dr. John Killen for providing his knowledge and help with the instrumentation, and experimental measurements. Dr. V.H. Arakeri, a visitor to S.A.F.H.L. during my stay, provided many helpful comments regarding theoretical and experimental aspects of this work.

I am indebted to my research partner, Mr. Jie Cheng, for his help in completing the experiments and also for offering his friendship so openly and with such enthusiasm.

Finally I would like to thank all the students and staff at S.A.F.H.L. for their help and friendship. It has made my stay at the lab not only educational, but fun.

This work was sponsored by the Office of Naval Research, Applied Research and Technology Directorate, Contract No. N00167-86-K-0054.

TABLE OF CONTENTS

	<u>Page</u>
ABSTRACT	i
ACKNOWLEDGEMENTS	ii
TABLE OF CONTENTS	iii
LIST OF SYMBOLS	v
LIST OF FIGURES	viii
LIST OF TABLES	x
1. INTRODUCTION	1
1.1 ACOUSTICS OF TWO-PHASE FLOWS	1
1.2 SCOPE OF WORK	2
2. BUBBLE CREATION NOISE	3
2.1 GENERAL	3
2.2 EXPERIMENTS	6
2.2.a FACILITY	6
2.3 RESULTS	8
2.4 DISCUSSION	11
2.4.a BUBBLE CLOSURE MODEL	13
2.4.b SURFACE TENSION EFFECTS	17
3. BUBBLE SPLITTING NOISE	19
3.1 GENERAL	19
3.2 EXPERIMENTS	21
3.2.a FACILITY	21
3.2.a.1 TURBULENCE AND NOISE MANAGEMENT	23
3.2.a.2 BUBBLE GENERATION	26
3.2.b MEASUREMENT AND ANALYSIS SYSTEM	29

TABLE OF CONTENTS (cont.)

	iv
	<u>Page</u>
3.3 RESULTS	32
3.4 DISCUSSION	37
4. CONCLUSIONS AND RECOMMENDATIONS	42
4.1 SUMMARY OF THIS INVESTIGATION	42
4.2 AREAS FOR FURTHER STUDY	44
REFERENCES	47
APPENDIX 1 : DESIGN OF A SCREENED DIFFUSER	50

LIST OF SYMBOLS

Symbol

C	a constant
C_d	coefficient of drag
C_p	coefficient of pressure
D	a diameter
D_b	bubble diameter
D_{crit}	bubble diameter at the critical Weber No.
D_n	nozzle (needle) diameter
E_k	kinetic energy
f_o	natural frequency - zero mode
g	gravitational acceleration
I	inertial coefficient
K	stiffness coefficient
L	a length
l	characteristic eddy length
M	the moment used in closing a bubble
m_{add}	hydrodynamic (added) mass of a bubble
m_b	mass of a bubble
P	a pressure
P_i	internal bubble pressure
P_{ref}	reference pressure - $1 \mu Pa$
P_o	static pressure in a liquid
P_+	excess pressure acting on a bubble
P_e	instantaneous external fluid pressure

SYMBOLS (cont.)

p_s	instantaneous sound pressure
p_o	sound pressure amplitude
R_b	bubble radius
R_n	nozzle (needle) radius
R_o	initial bubble radius
R	bubble wall velocity
r	distance or length
S	surface tension coefficient
s	coordinate along a path
t	time
t_s	characteristic time scale
U	velocity
U_j	jet velocity
U_r	relative velocity between a bubble and the jet
U_∞	free stream velocity
u'	characteristic velocity fluctuation
V_o	initial bubble volume
ΔV_o	instantaneous change in bubble volume
v	instantaneous bubble volume
\dot{v}	instantaneous volume velocity
\ddot{v}	instantaneous volume acceleration
$\overline{v^2}$	spatially correlated velocity over length scales on the order of a bubble diameter
W	work done against P_j to close a bubble
We_{crit}	critical Weber number for bubble splitting

SYMBOLS (cont.)

x_i	direction of stretching due pressure gradient
Z	resistive coefficient
γ	specific weight
δ	damping coefficient
ϵ	dissipation rate per unit mass
θ	angle bubble wall turns when closing
μ_f	dynamic viscosity of a fluid
π	3.14159
ϕ	phase angle
ρ	density
ρ_a	density of air
ρ_f	density of fluid
ρ_w	density of water
τ	shear stress
ω_0	circular natural frequency - zero mode

LIST OF FIGURES

<u>Figure</u>		<u>Page</u>
2.1	Schematic of the bubble creation test setup	7
2.2	Typical sound pressure signature - creation	8
2.3	Bubble diameter versus needle diameter	9
2.4	Bubble shape as a function of time	10
2.5	Peak sound pressure as a function of bubble size	11
2.6	Definition sketch of bubble closure model parameters	14
2.7	Comparison of peak sound pressures generated by three different methods	16
2.8	Effect of a change in local surface tension on the peak sound pressure of creation	18
3.1	Schematic of the experimental facility	22
3.2.a	Radial variation of the axial component of turbulent intensity at the nozzle exit plane	24
3.2.b	Longitudinal variation of the axial component of turbulent intensity along the jet centerline	25
3.3	Bubble sizes generated and critical bubble size for splitting versus jet velocity	29
3.4	Hydrophone location referenced to jet.	30
3.5.a	Typical waveform of a single bubble splitting event	31
3.5.b	Frequency spectrum of the waveform shown in figure 3.4 by FFT method	31
3.6.a	Bubble splitting waveform, $U_j = 2.7$ m/s	32
3.6.b	Bubble splitting waveform, $U_j = 5.0$ m/s	33
3.6.c	Bubble splitting waveform, $U_j = 7.5$ m/s	33
3.6.d	Bubble splitting waveform, $U_j = 10.0$ m/s	34

FIGURES (cont.)

<u>Figure</u>		<u>Page</u>
3.6.e	Bubble splitting waveform, $U_j = 12.5$ m/s	34
3.6.f	Bubble splitting waveform, $U_j = 15.0$ m/s	35
3.6.g	Bubble splitting waveform, $U_j = 17.5$ m/s	35
3.7.a	One-third octave band analysis of averaged spectra from single splitting events	36
3.7.b	One-third octave band analysis of background noise, no bubble injection	37
3.8	Deformation of bubbles in the shear layer of a submerged turbulent jet	38
3.9	Bubble splitting in the shear layer of the jet, $U_j=7.5$ m/s.	39
3.10	Initial period of bubble splitting noise waveform as a function of jet velocity	41
4.1	Acoustically excited bubble in quiescent water, from Hentschel and Lauterborn	46
A1.1	Final design for a wide-angle screened diffuser.	53

LIST OF TABLES

<u>Table</u>		<u>Page</u>
2.1	Comparison of peak sound pressures	15
A1.1	Design calculation for wide angle screened diffusers	52

CHAPTER 1

INTRODUCTION

1.1 ACOUSTICS OF TWO-PHASE FLOWS. The study of multiphase flows encompasses a large range of topics each with their related problems. In general, when a gas or vapor and a liquid coexist in a flowing system, elevated acoustic pressures can easily be generated. The increase in acoustic pressure may be attributed to several processes: such as bubble collapse, present in cavitation; or with turbulent excitation resulting in bubble oscillation and possible splitting in non-cavitating flows.

Past research in multiphase flow acoustics has been concentrated in the area of cavitation. This is mainly due to the intense, high acoustic pressures generated in a cavitating flow. These pressures can in turn cause severe damage to a variety of flow structures and equipment, including pumps and turbines. The use of noise as a parameter for studying cavitation has been widely used. Many researchers have used noise to identify cavitation inception for a large range of flow conditions. Some attempts have also been made to correlate noise with cavitation damage, Stinebring (1976). Much less research has been done on the acoustics of non-cavitating, two-phase flows.

The generation of elevated acoustic pressures in non-cavitating two-phase air-water mixtures has not been studied extensively. There are several applications, especially in the naval area where noise generation of this kind can be a highly undesirable condition. With the

advent of microbubble drag reduction technology and bubble screening techniques, interest in the noise that is generated if injected bubbles split in a turbulent flow is of interest. Other applications involving compressed gas bubbler systems may benefit from this type of research.

1.2 SCOPE OF THIS WORK. The work detailed within this thesis consists of two major parts, the study of:

- (1) noise generated due to formation and release of an air bubble from a nozzle in a tank of quiescent water, and
- (2) noise generated due to air bubbles splitting in the shear layer of a turbulent water jet.

The main body of this thesis deals with experiments carried out in these two areas. Noise measurements along with photographic investigations (stills and high-speed movies), provided insight into the noise generation mechanism. Some theoretical development along with recommendations for further research are given.

CHAPTER 2

BUBBLE CREATION NOISE

2.1 GENERAL. The creation of a gas bubble in a liquid can result in the generation of a sound pulse. The noise is a direct result of the motion of the bubble wall, and in particular the zero mode or simple volume oscillation, Strasberg (1956). When a bubble is formed the noise is produced by an internal or external pressure difference acting on the bubble wall. The resulting noise is thus a function of the method used to create the bubble. Creating gas bubbles by electrolysis for instance results in noise of a smaller amplitude than creation of a gas bubble at an orifice or nozzle.

Minnaert (1933), was the first to investigate bubble generation at a nozzle. He crudely measured the natural frequency of bubble oscillation and found the dominant frequency followed the relationship,

$$f_0 = \frac{(3\gamma P_0 / \rho)^{\frac{1}{2}}}{2\pi R_b}, \quad (2.1)$$

where P_0 is the static pressure in the fluid and R_b is the bubble radius. This concept was taken a step further by Strasberg (1956) where he compared relative noise production caused by oscillation at the first four symmetric modes of vibration. From a theoretical procedure detailed by Lamb (1945), it was shown that the zero mode is the dominate one in producing sound (acoustic pressures are 10^6 times greater than those generated by the second or third modes). With this

information, the investigations can be limited to the simple volume pulsations (zero mode).

In addition to the bubble oscillating at a frequency dependent on its size, dissipation of the oscillating acoustic pressure takes place. The major influences present in the damping are; thermal, acoustic radiation, and viscous effects. Devin (1959) presented a value for the total damping coefficient which is made up of the contributions of each of the individual effects. For bubbles larger than 0.1 mm in diameter, the viscous damping effects can be ignored and the resulting coefficient is,

$$\delta = 0.014 + 4.5 \times 10^{-4} f_0^{\frac{1}{2}} \quad (2.2)$$

Meyer and Skudryzk (1953) have also presented work on damping and gave a coefficient based on experimental results equal to,

$$\delta = 0.014 + 1.1 \times 10^{-5} f_0 \quad (2.3)$$

Theoretically, the damped sinusoidal oscillation is a result of a pulsating sphere in a dissipative fluid. Basic hydrodynamics can give some ideas about the noise production. Assuming the bubble wall movement is small in comparison to the bubble radius (small perturbation), the motion can be described by the conventional second-order linear differential equation,

$$I\ddot{v} + Z\dot{v} + K(v - V_0) = P_0 - p_e(t), \quad (2.4)$$

with the initial conditions, $(v(0) - V_0) = \Delta V_0$ and $\dot{v}(0)$, where v is

the instantaneous bubble volume. In this equation, I , Z , and K are inertial, resistive, and stiffness coefficients, respectively; P_0 is the pressure at which the bubble has a volume V_0 ; $p_e(t)$ is the instantaneous external pressure which would exist in the liquid if the bubble were not there; and the dots denote the first and second derivatives with respect to time. The coefficients are given by, $I = \rho/4\pi R_0$ and $K = \gamma P_0/V_0$, Z depends on both the bubble size and frequency in a complicated way. Also, assuming that the sound and external pressure fields are uniform around the bubble wall and large enough that surface tension and heat transfer out of the bubble can be neglected, then the instantaneous sound pressure radiated by the bubble at a distance r is,

$$p_s = \frac{\rho \ddot{v}}{4\pi r} \quad (2.5)$$

Volume pulsations are initiated when the external pressure p_e , departs from the static value P_0 . If this departure is of very short duration, the major interest is in the oscillations which continue after the external pressure has returned to the static value. In this case the right side of equation 2.4 is set equal to zero and the solution results in,

$$p_s = p_0 e^{-(\rho f_0 \delta t)} \cos(2\pi f_0 t - \phi), \quad (2.6)$$

using $\omega_0 = 2\pi f_0$, the amplitude of the sound pressure, p_0 , is,

$$p_0 = (\rho \omega_0^2 / 4\pi r) [\dot{v}^2 + \omega_0^2 (v(0) - V_0)^2]^{\frac{1}{2}} \quad (2.7)$$

Following are the details of a set of experiments used to study these concepts further.

2.2 EXPERIMENTS. A series of experiments were designed to measure the sound pressure signal produced by the formation and release of an air bubble in quiescent water. The major topics of interest were: the noise generation mechanism, peak sound pressure amplitudes, bubble size determination by frequency, and damping characteristics of the acoustic signal.

2.2.a Facility. The experiments were carried out in a rectangular (508 mm by 254 mm by 304 mm) acrylic tank filled with distilled water. Air bubbles were created by passing dry, compressed air through hypodermic needles of various sizes. The air pressure was regulated to 27.5 kPa gauge, and the air flowrate was controlled and measured by a combination needle valve-rotameter assembly. Five different needle sizes were tested; 18, 21, 25, 27, and 31 gauge, which corresponded to 0.838, 0.508, 0.254, 0.203, and 0.152 mm I.D., respectively. The water temperature and atmospheric pressure were recorded for each test.

The sound pressure was measured using a B & K Model 8103 miniature piezoelectric hydrophone. The hydrophone output was passed through a B & K low noise amplifier (40 dB gain) and into a Wavetek analog antialiasing filter. The filter was configured to pass frequencies between 500 and 100,000 Hz. An additional 40 dB of gain could be applied, if needed, by the filter. The filtered output then was input into a Nicolet Model 4094 high-speed digital oscilloscope. The sound pressure waveforms were captured by the oscilloscope, and provided up

to 15,872 digitized points per waveform, taken at rates up to 2MHz. The stored waveforms were then transferred to a IBM-AT micro-computer for data storage and further analysis. A schematic of the experimental setup is shown in figure 2.1.

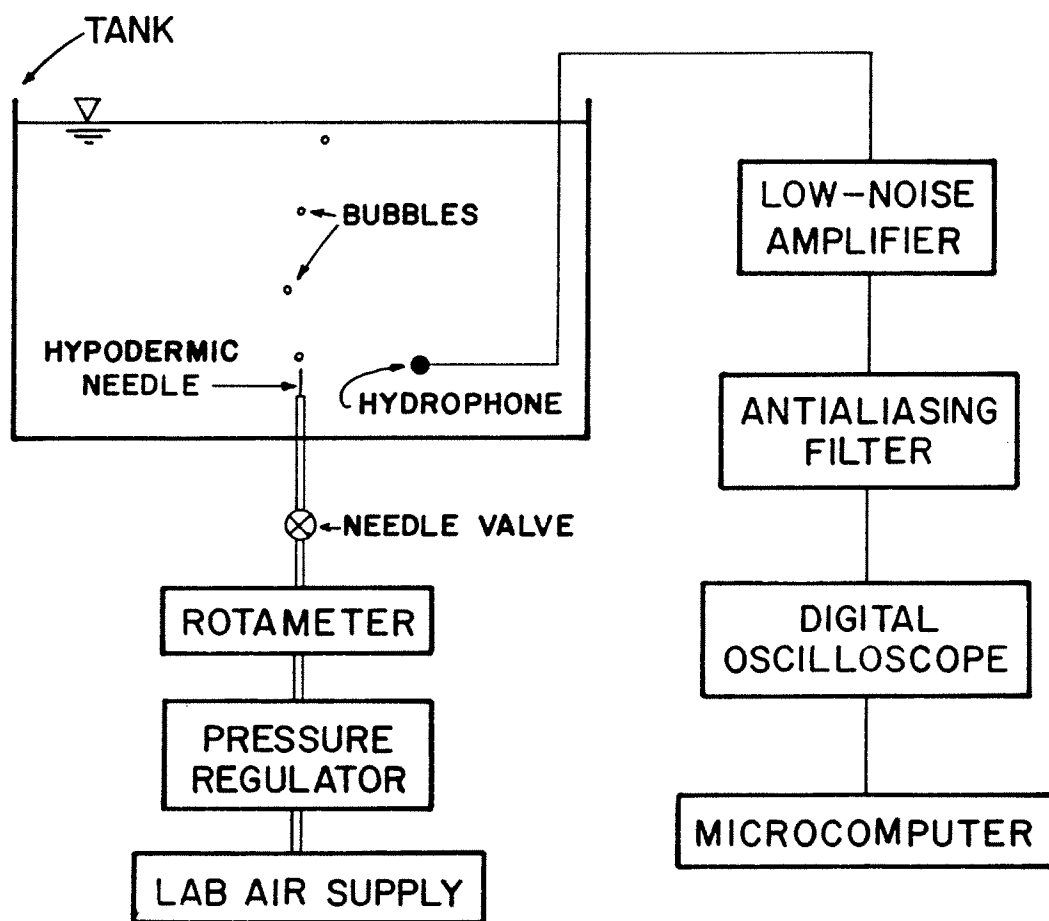


Figure 2.1. Schematic of bubble creation test setup.

2.3 RESULTS. As other researchers have found, the acoustic pressure waveform of bubble formation at a nozzle is characterized by a damped sinusoidal oscillation, figure 2.2.

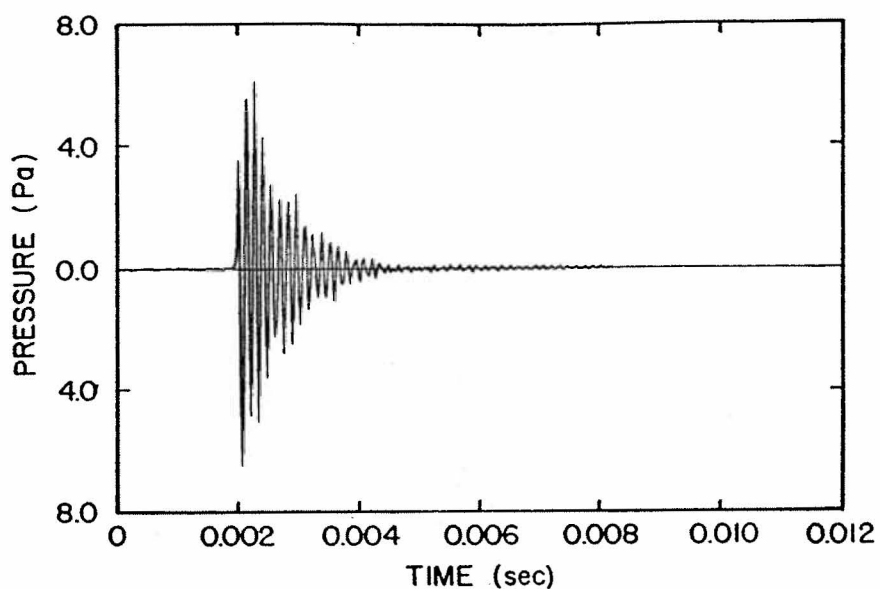


Figure 2.2. Typical sound pressure signature.

Each transient waveform was analyzed for its peak sound pressure level as well as its frequency components.

The frequency analysis was carried out with a FFT (Fast Fourier Transform) algorithm programmed and run on the microcomputer. In each case, the FFT was run on a time series of 8192 points. Data acquisition rates were 200 kHz. The analysis yielded: that the bubbles oscillate at their zero mode natural frequency, which is constant for

a particular bubble size. Comparisons with measurements of bubble diameter by photographic methods agreed well with bubble sizes predicted by equation 2.1 using the frequencies measured experimentally. The variation of bubble diameter with needle diameter is shown in figure 2.3

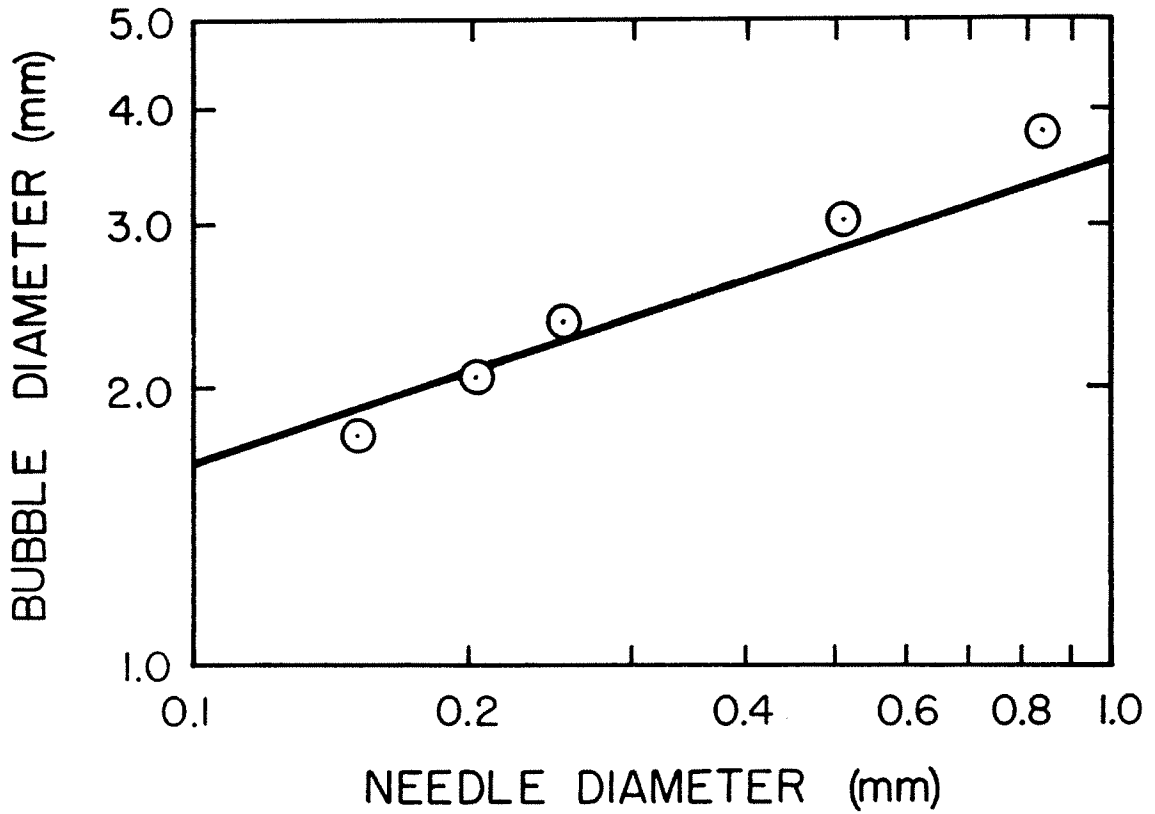


Figure 2.3. Bubble diameter versus needle diameter.

The peak sound pressure was picked out of each waveform, and usually was the second or third peak of the oscillation. A photographic summary of a typical waveform is shown in figure 2.4. Here the bubble is shown during different points throughout the sound producing time of its rise.

Figure 2.4. Bubble shape as a function of time.

The peak sound pressure levels over the range of bubble sizes tested are shown in figure 2.5. These levels are averages of many bubbles created in each size range.

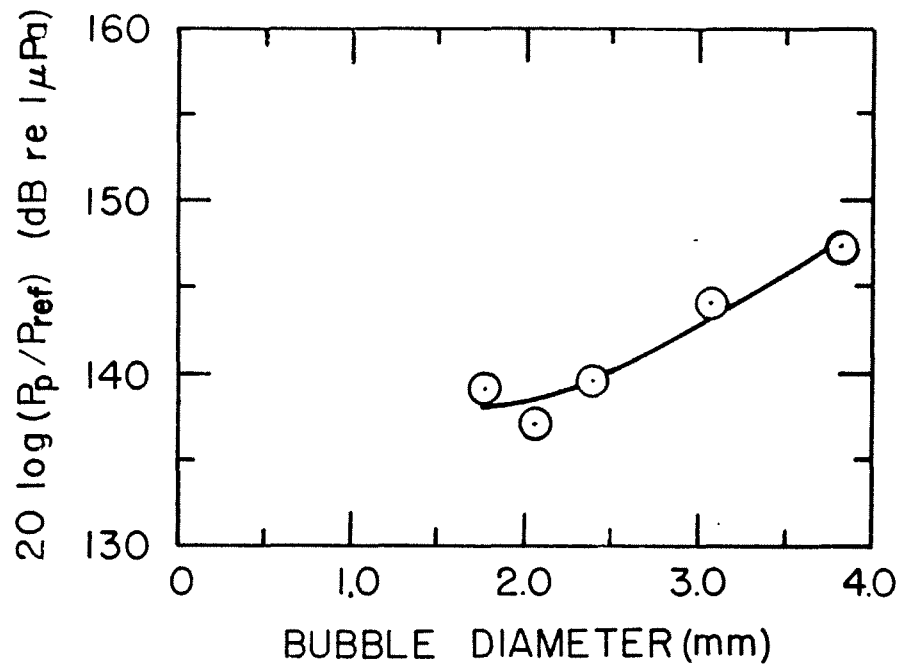


Figure 2.5. Peak sound pressure as a function of bubble size.

2.4 DISCUSSION. The theory detailed by Strasberg does not fully agree with the experimental data presented in this thesis. Minnaerts' equation of natural frequency agreed well, when bubbles sized from photographs, were compared to their size predicted from frequency measurements (figure 2.3). The decay envelope describing the damping present also agreed satisfactorily with the results presented by Meyer and Skudryzk. The major discrepancy was in the comparison of the measured and predicted values of peak sound pressures.

Equation 2.4 correctly describes the bubble motion, however, the pressure amplitude is determined largely by the initial conditions used to solve the equation. In Strasbergs' development, he assumes that the pressure inside the bubble, P_i , is a constant and is equal to the static pressure in the fluid plus the surface tension pressure required to grow a bubble. This excess pressure, P_+ , remains constant throughout the very slow bubble growth. Using these assumptions, the volume velocity at separation is approximately,

$$\dot{v}_0 = 4\pi R_0^2 (2P_+/3\rho)^{\frac{1}{2}}. \quad (2.8)$$

The bubble volume can be approximated as,

$$(v(0) - V_0) = V_0 (P_+/P_0). \quad (2.9)$$

The term involving $(v(0) - V_0)$ in equation 2.7 is generally small and can be neglected. Substituting equation 2.8 into equation 2.7, the peak sound pressure at a distance r is,

$$p_0 = (R_0/r) (2\gamma P_0 P_+)^{\frac{1}{2}}. \quad (2.10)$$

When using this equation to calculate peak sound pressures for bubbles of equal size to the present experiments, the values were on average 40 dB greater than the measured pressures.

If the theory is to approach the measured values, the volume velocity needs to be much smaller. Strasberg presents a measurement of the volume velocity taken from high speed movies, which is more than one order of magnitude smaller than what equation 2.8 predicts.

However, never formally addresses this anomaly and finally just disregards the measured value when presenting his conclusions.

A review of the assumptions leads one to question the validity of whether the bubbles' internal pressure remains constant throughout formation, growth, and detachment. The excess pressure, P_+ , initially must be $2S/R_n$ to begin bubble formation, where S is the surface tension coefficient and R_n is the nozzle radius. However, as the bubble grows, the magnitude of P_+ may decrease since much less pressure is required to sustain the growth. If the excess pressure decreases until the moment of detachment, then the bubble wall velocity decreases, resulting in a much smaller peak sound pressure.

2.4.a Bubble Closure Model. The need for a different model to predict the peak sound pressure is evident. By taking an energy approach, the formation of a bubble on a nozzle and its detachment can be looked at more closely. As the bubble detaches from the nozzle, work is done against P_+ to close the bubble. This work is then transformed into kinetic energy in the resulting oscillation. If these two quantities are equated, a new value of the volume velocity can be calculated. The work can be defined as,

$$W = M \theta \quad (2.11)$$

where M is a moment further defined as,

$$M = \iint_A P \cdot s \, dA = 2\pi R_n P \int_0^{R_n} s \, ds = \pi R_n^3 P. \quad (2.12)$$

Substituting the surface tension pressure for P , this gives the final

relationship for the closure work,

$$W = \pi R_n^3 (2S/R_b) \theta, \quad (2.13)$$

in terms of important parameters, figure 2.6.

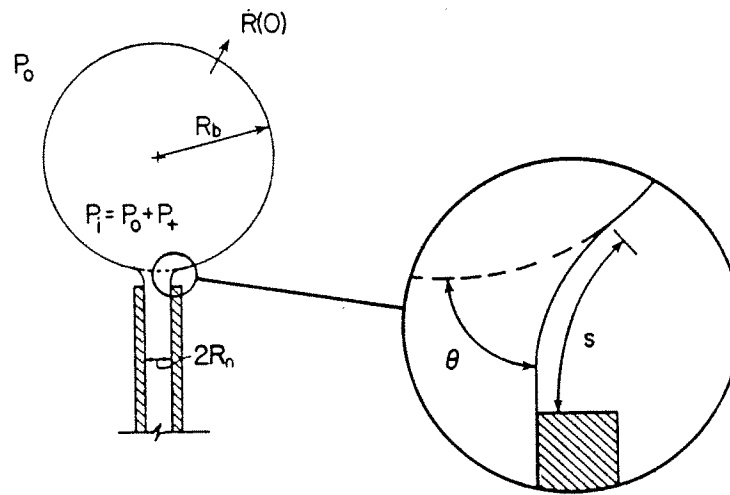


Figure 2.6. Definition sketch of bubble closure model parameters.

This work is then converted into kinetic energy in the resulting oscillation. The kinetic energy is given by,

$$E_k = \frac{1}{2} (m_b + m_{\text{add}}) \dot{R}^2 \quad (2.14)$$

The added mass term, accounts for the acceleration of the fluid surrounding the pulsating bubble. Milne-Thompson (1960), has calculated m_{add} to be $4\pi R_b^3 \rho_w$. Compared to the mass of the bubble, $m_b = 4/3\pi R_b^3 \rho_a$, the added mass term is (≈ 3000 times larger). If the mass of the bubble is neglected,

$$E_k \approx 2\pi\rho R_b^3 \dot{R}^2 \quad (2.14a)$$

Now equating the work to the kinetic energy, and solving for the initial bubble wall velocity,

$$\dot{R} = \left(\frac{R_n}{R_b} \right)^{3/2} \left(\frac{S\theta}{\rho R_b} \right)^{1/2}, \quad (2.15)$$

or in terms of the initial volume velocity,

$$\dot{v}(0) = 4\pi R_b^2 \dot{R} = 4\pi R_n^2 \left(\frac{S\theta}{\rho} \right)^{1/2}. \quad (2.15a)$$

This expression can now be used to calculate the initial condition used in solving equation 2.4. Results showing measurements, Strasbergs theory (equation 2.10), and the closure model, are shown in Table 2.1 and figure 2.7. The dip in the measured pressure curve, figures 2.5 and 2.7, can not be explained through any physical arguments. The bubble size progresses as expected; however, the drop in sound pressure noted with the 0.203 mm diameter needle is unexplained.

TABLE 2.1 Comparison of peak sound pressures.

Needle size (mm I.D.)	Bubble size (mm dia.)	P _{meas}	P _{theory}	P _{model}
		(dB re 1 μPa)		
0.838	3.812	147.3	179.4	153.5
0.508	3.048	143.9	179.6	148.9
0.254	2.370	139.6	180.5	142.1
0.203	2.052	137.1	180.2	140.4
0.152	1.778	139.1	180.2	137.9

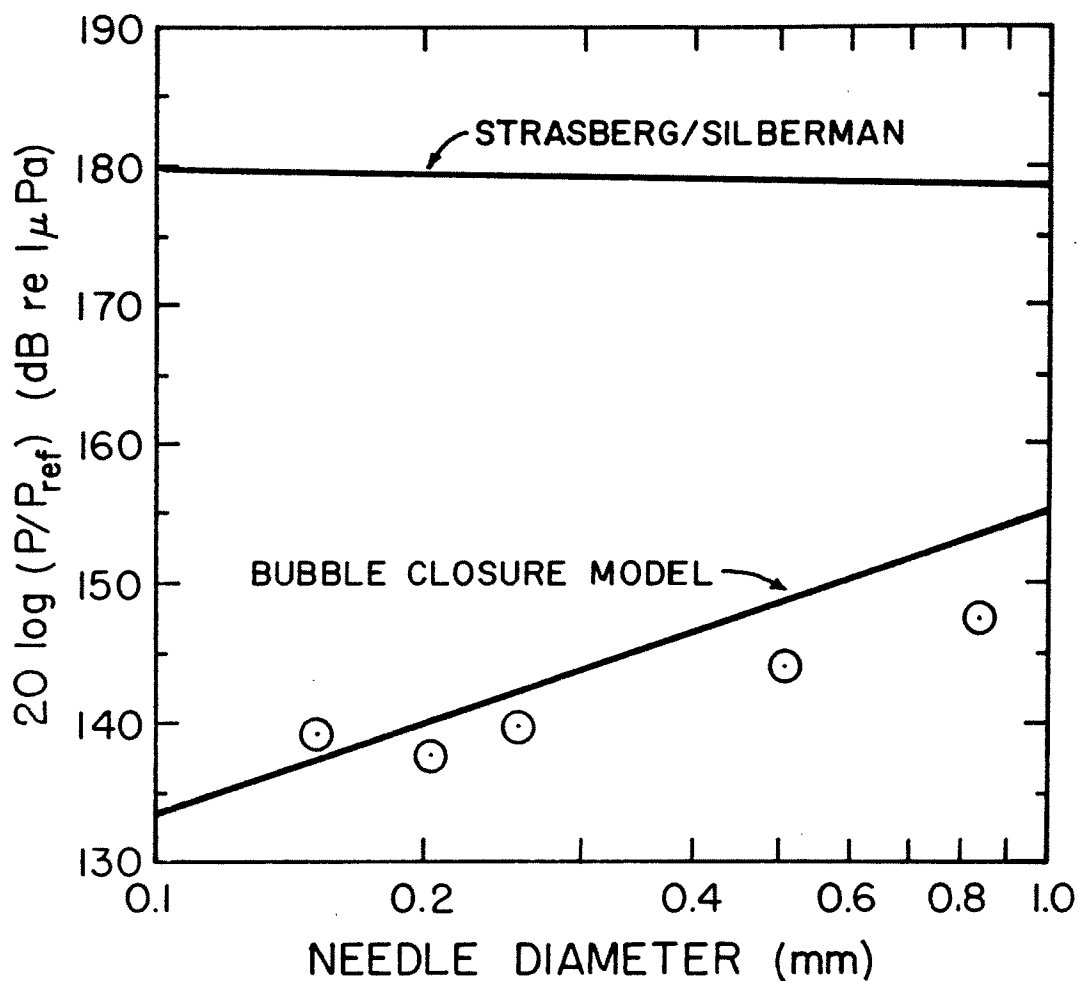


Figure 2.7. Comparison of three values of peak sound pressure.

The results of the closure model and experiments agree within 3 to 6 dB, however, the theoretical value (from Strasberg), gives results 40 dB too high. The major difference in the closure model and Strasbergs' theory is in the expression for the initial bubble wall velocity. Basic hydrodynamic theory does not account for the complex balance of

forces which are present at the formation of an air bubble at a nozzle when submerged in water. The large discrepancy shows the importance of using physically correct initial conditions when solving equation 2.4.

2.4.b. Surface Tension Effects. Although the above work is the major interest in this thesis, another interesting feature concerning bubble creation at a nozzle was discovered. The bubble closure model emphasizes the importance of the effect of surface tension on the initial bubble volume velocity with its strong dependence on the angle of attachment and the surface tension coefficient. The effect of a change in localized surface tension produces an interesting result concerning sound pressure amplitudes. A thin coating of oil was placed on the needle and bubbles were created identically as before. A slight increase in bubble diameter was noted as might be expected due to the increase in the localized surface tension coefficient, however, a decrease in the peak sound pressure of approximately 10 dB was also noted, figure 2.8. This trend is opposite of what the experimental results of the previous tests predict. The prior experiments generally show an increase in sound pressure with an increase in bubble diameter. One hypothesis that might explain the decrease in sound pressure follows. The sound pressure is dependent on the angle, θ , that the bubble wall is attached to the nozzle with. As the surface properties of the nozzle change, this angle will change. Depending on the magnitude of the surface tension coefficient S , if the angle is decreased, the sound pressure will also decrease. A strict analytical treatment of this phenomenon quickly becomes a complex problem in

interfacial physics. It could be possible to substantially decrease the sound pressure generated by bubble creation at orifices and nozzles by simply varying the material used to form the orifice or nozzle. This feature could have important implications in many areas.

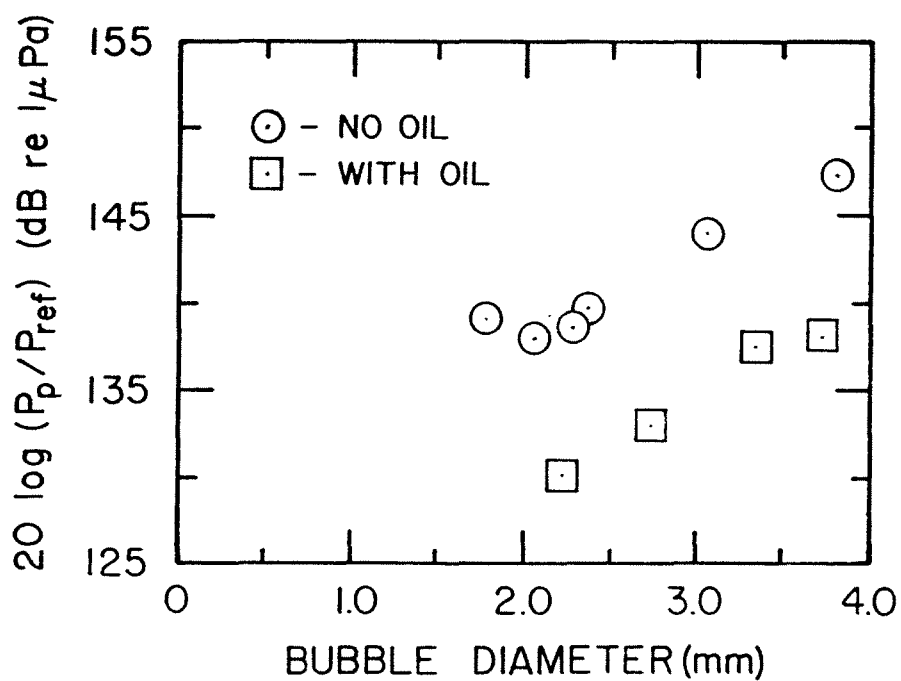


Figure 2.8. Effect of a change in local surface tension on the peak sound pressure.

CHAPTER 3

BUBBLE SPLITTING NOISE

3.1 GENERAL. The generation of noise due to bubble splitting has many similarities with bubble creation noise. The foremost being that the bubbles which result from the splitting, oscillate in one or a combination of their fundamental modes, emitting noise at frequencies related to the bubble size. In general however, splitting noise is a highly complex phenomena, especially when the excitation forcing the splitting is a turbulent flow field.

Strasberg (1956) was one of the first to address the noise associated with bubble splitting. In a quiescent flow, he proposed that bubble splitting noise should be equivalent to the noise of bubble coalescence. When the splitting occurs in a turbulent shear flow, this premise does not hold. Only a few experimental works exist on the subject of gas bubbles splitting in turbulent liquid flows. Gavigan, et. al. (1974) and Blake (1976) both took measurements of bubble splitting noise in turbulent wakes. Killen (1982) made similar measurements in the turbulent boundary layer of a flat plate.

The experiments detailed in this thesis concern the splitting of single air bubbles which have been injected into the potential core of a turbulent water jet. There are several types of noise generating mechanisms present in this type of flow. Turbulent jet noise has been studied at great length. In a single phase jet, the noise is characteristic of the turbulence, and behaves as an acoustic quadrupole.

When a second phase is introduced, either monopole or dipole behavior is observed. The case of air bubbles in a turbulent water jet results in a combination of monopole and quadrupole sound sources. Blake (1984) gives a very complete bibliography of works concerning jet noise.

Two-phase jet noise has received less attention than single-phase, however a few works do exist. Crighton and Ffowcs-Williams (1969) have presented an analytical development on noise generated by two-phase air-water jets, and Whitfield and Howe (1976) have performed a set of experiments in this same area. In a somewhat related area, a number of studies on jet cavitation noise have been done. Jorgensen (1958) was perhaps the first to study the spectra of acoustic pressure generated in a cavitating jet. Recently, Ooi (1981), Taghavi (1985), and Franklin and McMillan (1984) have all performed experimental and analytical studies of jet cavitation. Franklin (1985), has even related many features of the noise of a cavitating jet to the flow structure of a single-phase jet. The question still remains whether splitting noise in a non-cavitating two-phase jet flow has any similarities.

While almost no research has been done on bubble splitting acoustics, quite a number of works exist concerning the actual mechanics of bubble deformation and splitting. The majority of these studies have dealt with the interfacial instability problem, and have concentrated on the forces acting on the interface. Hinze (1955) was the first to publish work on drop and bubble deformation in turbulent flow fields. Many others since have extended his work, including Collins and Knudsen (1970), Sevik and Park (1973), Han and Funatsu (1978), and most re

cently Bentley and Leal (1986). Ooi and Acosta (1984) have related microbubble deformation to the fluctuating pressure gradients present in a submerged jet flow. Hentschel and Lauterborn (1985) have used high-speed holograms to detail the breakup of an air bubble driven to instability and splitting by acoustic radiation.

While a fair understanding of bubble splitting mechanics exists for finely controlled flow fields, not many real world applications have been studied. In addition, the topic of noise generation by the splitting event has scarcely been studied at all.

3.2 EXPERIMENTS

A series of experiments were run to investigate the noise due to bubble splitting in a turbulent free shear flow. The research, carried out at the St. Anthony Falls Hydraulics Laboratory, utilized an existing test facility.

3.2.a Test Facility

The test facility used in these experiments was originally designed to study cavitation characteristics in a free shear layer, Taghavi (1985). It included a high-head pump driven by a 20-horsepower motor; a test section, 0.61 m in diameter and 1.5 m long which housed a 25.4 mm diameter nozzle used to create a jet. The submerged jet, capable of velocities up to 30 m/s, issued vertically into this tank and was momentum conserving within 1-percent throughout the measurement region. The ambient pressure in the tank could be controlled between 0.1 atm and 2 atm. A heat exchanger on the return piping stabilized the fluid temperature. Flexible couplings provided vibration isolation to

the test section. Jet velocity was monitored using a differential transducer to measure the pressure drop. The nozzle had been calibrated with a laser velocimeter. Free gas content of the water could be controlled by operating the tank at a reduced pressure for varying lengths of time, figure 3.1.

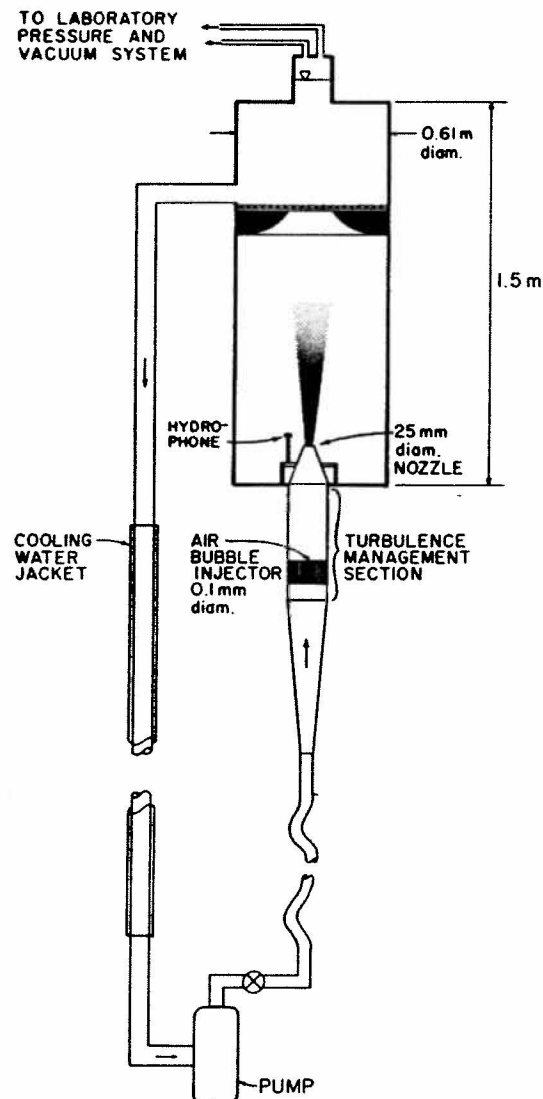


Figure 3.1. Schematic of the experimental facility.

Several modifications to this facility were needed to perform the

present experiments. These are detailed in the following sections.

3.2.a.1 Turbulence and Noise Management

The initial turbulence level in the jet and the ambient noise levels were both important considerations in the experimental work. Low turbulence was desired to insure that when bubbles were injected into the flow, splitting would occur only in the free shear layers created by the jet flow and not within the nozzle or the jets' potential core. In addition, the background noise levels of the facility while operating had to be low enough to detect bubble splitting with the hydrophone located in the test section.

The addition of a bubble injecting apparatus forced a change in the existing turbulence management section, Taghavi (1985). The new arrangement included a honeycomb followed by a fine mesh wire screen. The honeycomb was made from plastic drinking straws, packed without deformation of the circular cross-section. The average inside diameter of a cell was 5.4 mm with a wall thickness of 0.15 mm. The cell length was 108 mm, giving an L/D ratio of 20. The hypodermic needle used to create air bubbles, was located in the center cell of the honeycomb with an air supply line crossing the entrance of the honeycomb.

An analysis due to Batchelor (1970), and further detailed in Lumley and McMahon (1967), predicted that use of a 40-mesh screen (or smaller) would result in a turbulent intensity of 0.1-percent at the nozzle exit. This value assumes the turbulence decay length present in this facility along with an incoming turbulent intensity of 20-percent. A 50-mesh bronze wire screen was placed at the exit of the honeycomb.

Loehrke and Nagib (1976) and Scheiman (1981) have both shown the value of placing a screen directly downstream from the honeycomb in order to break up the laminar shear layers which develop in large L/D ratio honeycombs. The screen also decreases the eddy sizes present in the flow into a more dissipative size range.

Measurements of the axial components of velocity fluctuations in the jet were taken with a 3W Argon-ion laser doppler velocimeter. Measurements were taken across the center plane of the nozzle exit as well as along the jets centerline through the developing region of the jet. Measurements were taken before and after the honeycomb modifications discussed above, figure 3.2, a and b. There is a slight improvement in the turbulence levels with the modified honeycomb.

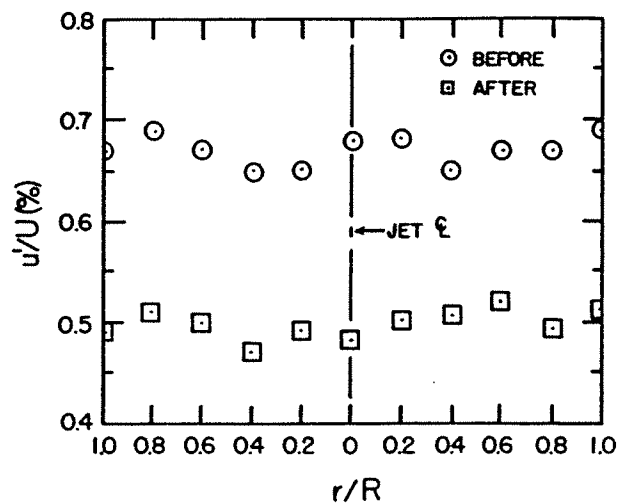


Figure 3.2.a. Radial variation of the axial component of turbulent intensity at the nozzle exit plane.

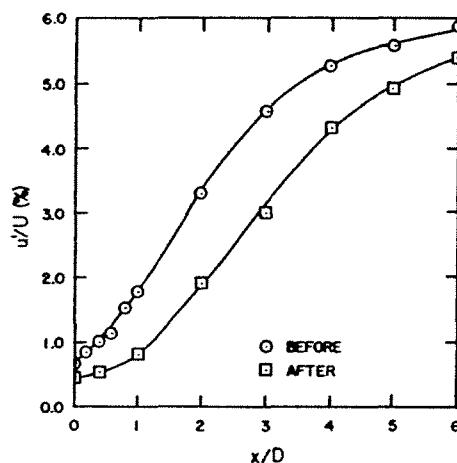


Figure 3.2.b. Longitudinal variation of the axial component of turbulent intensity along the jet centerline.

However, the desired level of 0.1-percent was not reached. This was largely due to the diffuser which was located directly upstream of the honeycomb. The wide-angle diffuser had a half angle of 4.76° , which suggests that separation could easily occur within the diffuser depending on the back pressure. Separation can cause random, highly turbulent bursts to enter the honeycomb, with turbulent intensities well above 20-percent. A screened wide angle diffuser was designed but not installed for these experiments due to time and budget constraints, see Appendix 1 for diffuser design procedure.

The ambient noise levels in the closed loop system were initially too high to adequately measure splitting events. The 20 horsepower motor driving the pump used to recirculate the flow, along with a 50.2 mm gate valve used to throttle the flow were located approximately 7 m from the test section. The motor operated at 3600 r.p.m., which was

within the frequency range of interest for the noise measurements. Since the speed of the motor could not easily be controlled, the pump and motor were moved away from the measurement location and an additional 25 m of piping was added to both the discharge and suction sides of the pump. The increased friction slightly reduced the maximum velocity available at the test section but at a jet velocity of 20 m/s, the operating noise level was reduced by 20 to 35 dB. This decrease in the ambient noise allowed for measurement of bubble splitting events and even made bubble creation noise measurable. Moving the pump and motor made it possible to measure the noise in a frequency band between 1- and 100-kHz. In addition, measurements were taken at night when common background noise from the work environment was at a minimum.

3.2.a.2 Bubble Generation

Since the major emphasis of this project was to investigate noise due to bubble splitting, design of a bubble generating device was important. Several methods of bubble creation were researched. The review concluded that even though extremely small bubble sizes were possible through electrolysis and chemical reaction, the highest level of repeatability of size and control of generation rate, was accomplished by forcing gas through an orifice or nozzle (needle).

Bubble creation at an orifice (needle) in quiescent water is governed by a balance of the forces acting on the bubble. The buoyancy force must overcome the surface tension force, yielding,

$$D_b = \left(\frac{6SD_n}{\rho_f g} \right)^{1/3}, \quad (3.1)$$

where D_b is the bubble diameter, D_n is the needle diameter, S is the surface tension coefficient, and ρ_f is the density of the liquid state. However, when the bubble detachment is aided by a relative flow past the bubble (the jet), the drag force must also be included in the balance. This results in,

$$D_b = \left(\frac{8SD_n}{C_d \rho_f U_r^2} \right)^{\frac{1}{2}}, \quad (3.2a)$$

where C_d is the drag coefficient and U_r is the relative velocity of the liquid. The drag coefficient, C_d , for a nearly spherical bubble and a Reynolds number of 10^3 to 10^5 , is approximately 0.5,

Silberman (1957). Given our geometry, the relative velocity, $U_r = 0.027U_j$, where U_j is the mean jet velocity in the test section. Substituting into equation 3.2a, we get,

$$D_b = \left(\frac{8SD_n}{\frac{1}{2}\rho_f (.027U_j)^2} \right)^{\frac{1}{2}}. \quad (3.2b)$$

Hinze (1955) produced some of the first work relating to the splitting of drops and bubbles. He derived the critical condition for bubble splitting. His condition stated that for splitting, τ , a surface force per unit area should obey the following,

$$\tau > (S + \mu_a(\tau/\rho_a)^{\frac{1}{2}})/D_b, \quad (3.3)$$

where $\mu_a(\tau/\rho_a) / D_b$ is the viscous stress. In a turbulent flow, the viscous stresses are not as important as the dynamic pressures and can be neglected. This results in $\tau > S/D_b$, and τ is of order $\rho \overline{v^2}$,

where $\overline{v^2}$ is the spatial average of the squares of the velocity differences over a distance equal to D_b . Hinze formed a critical Weber number based on these concepts,

$$We_{crit} = \frac{\rho \overline{v^2} D_{crit}}{S}, \quad (3.4)$$

where D_{crit} is the bubble diameter at the critical Weber number. In other work, Sevik and Park (1973), built on Hinzes' theory and came up with the critical Weber number for a turbulent jet. A value of $We_{crit} = 1.24$ was found theoretically and $We_{crit} = 1.3$, experimentally. If we consider isotropic turbulence, Batchelor (1951), shows that,

$$\overline{v^2} = 2(\epsilon D)^{2/3}, \quad (3.5)$$

where ϵ , is the turbulent energy dissipation rate. Assuming viscous effects to be dominated by surface tension effects,

$$D_{crit} = \left(\frac{\rho_f}{S} \right)^{3/5} \epsilon^{2/5} = C, \quad (3.6)$$

or,

$$D_{crit} = C \left(\frac{S^3}{\rho \epsilon} \right)^{1/5}, \quad (3.7)$$

where C is a constant dependant on the type of flow field, i.e. boundary layer, jet, etc. Sevik and Park calculated $C=1.15$ for a jet. With the range of sizes available in hypodermic needles, the bubble size created as a function of jet velocity, can be plotted. If the critical bubble size for splitting is also plotted, the experimental range of the test facility is revealed. By varying only the jet velocity, a

single bubble can pass from a non-splitting into a splitting regime, figure 3.3.

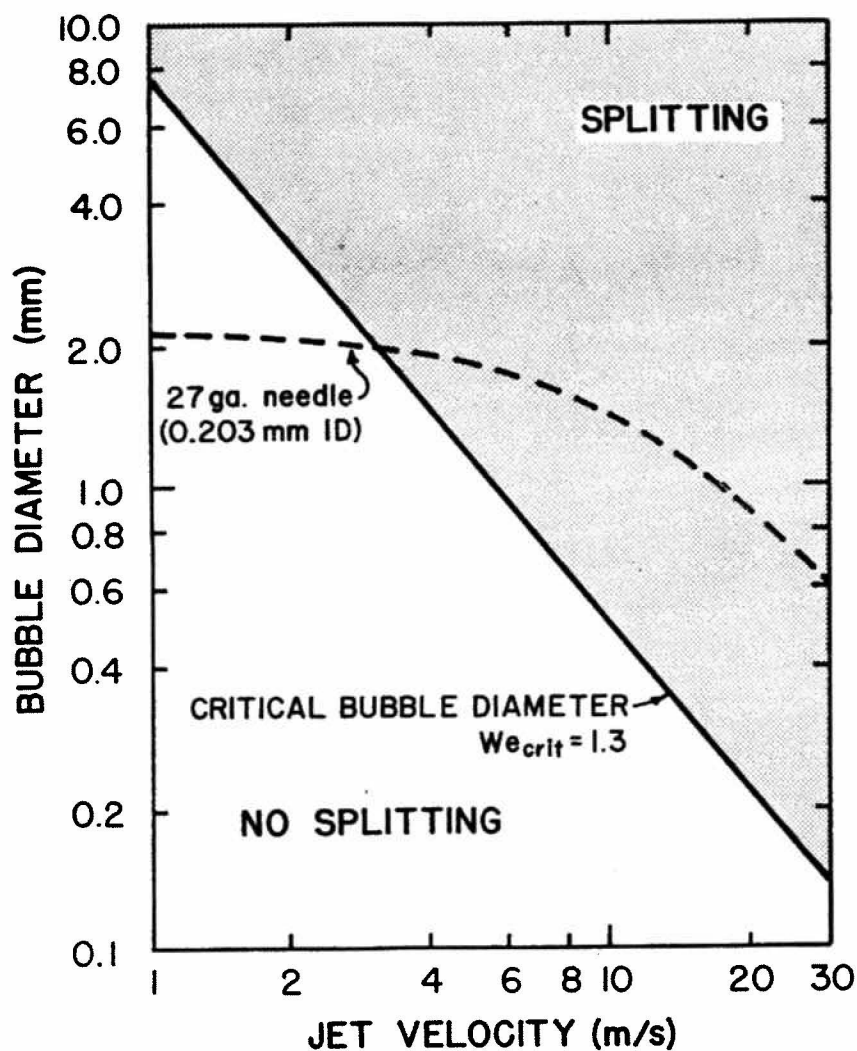


Figure 3.3. Bubble size generated by hypodermic needle with critical bubble size for splitting, versus jet velocity.

3.2.b Measurement and Analysis System

The noise measurements were made with a B & K Model 8103 miniature piezoelectric hydrophone mounted inside the test section, four jet

diameters downstream of the nozzle exit and four jet diameters off the jet centerline, figure 3.4. This location was chosen due to numerous previous studies where measurements of jet noise were taken, Jorgensen (1960), and Franklin (1985). The hydrophone output was input into a low noise amplifier where 40 dB was added to the signal. From this point, the signal was bandpass filtered at 1- to 100-kHz with a Wavetek analog filter. The filtered output was then input into a Nicolet Model 4094 high-speed digital oscilloscope, which stored 15782 digitized points per waveform at rates up to 2 MHz. Each test run consisted of a waveform of 8192 points taken at a rate of 250 kHz. These captured waveforms were then transferred to a IBM-AT microcomputer for storage and further analysis.

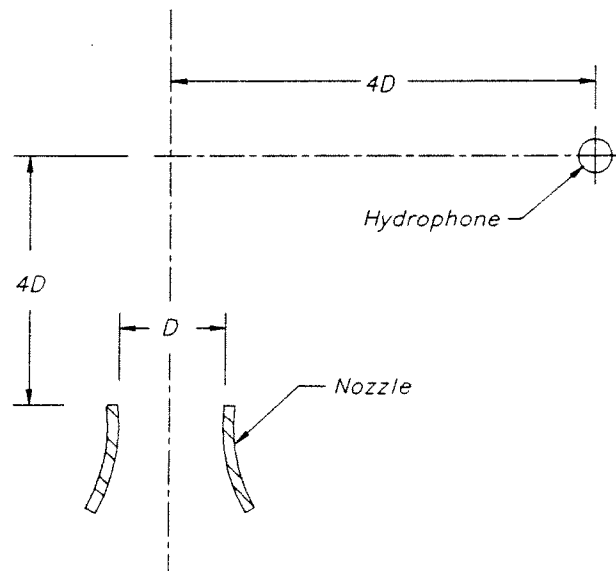


Figure 3.4. Hydrophone location referenced to jet.

The bubble splitting waveforms, figure 3.5.a, were analyzed in several different ways. Fourier analysis was performed to determine the frequency components of each transient waveform, figure 3.5.b

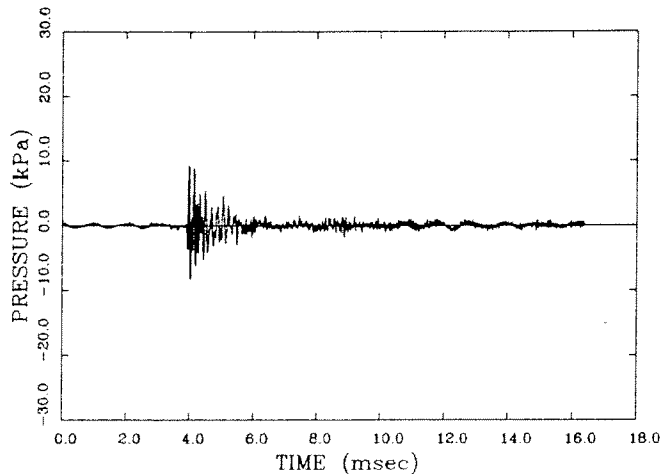


Figure 3.5.a. Typical waveform of a single bubble splitting event.

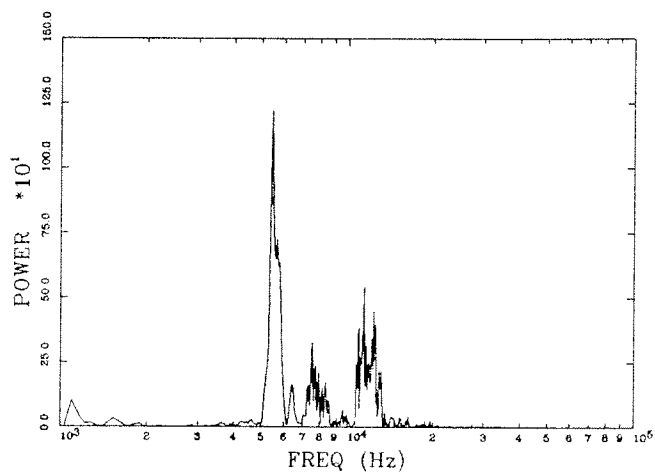


Figure 3.5.b. Frequency spectrum (power) of the waveform shown in figure 3.5.a by FFT method.

This was accomplished by performing a FFT (Fast Fourier Transform) on the recorded waveforms. The algorithm was coded in a FORTRAN program, and run on the microcomputer. In addition, 1/3 octave band analysis was performed. Analysis of the actual time series also yielded some interesting results.

3.3 RESULTS

A series of bubble splitting events were collected for jet velocities of 2.7, 5.0, 7.5, 10.0, 12.5, 15.0, and 17.5 m/s. A sample of a splitting waveform for each jet velocity is shown in figure 3.6, a-g. In each case, the bubbles were generated one at a time, using a 27-ga. Hypodermic needle (0.2 mm I.D.).

As with the bubble creation experiments, each waveform was analyzed for its frequency content. One-third octave analysis was performed on averaged spectra for each jet velocity tested. In each case, sixteen splitting events were used to assimilate the average spectra, figure 3.7.a and 3.7.b.

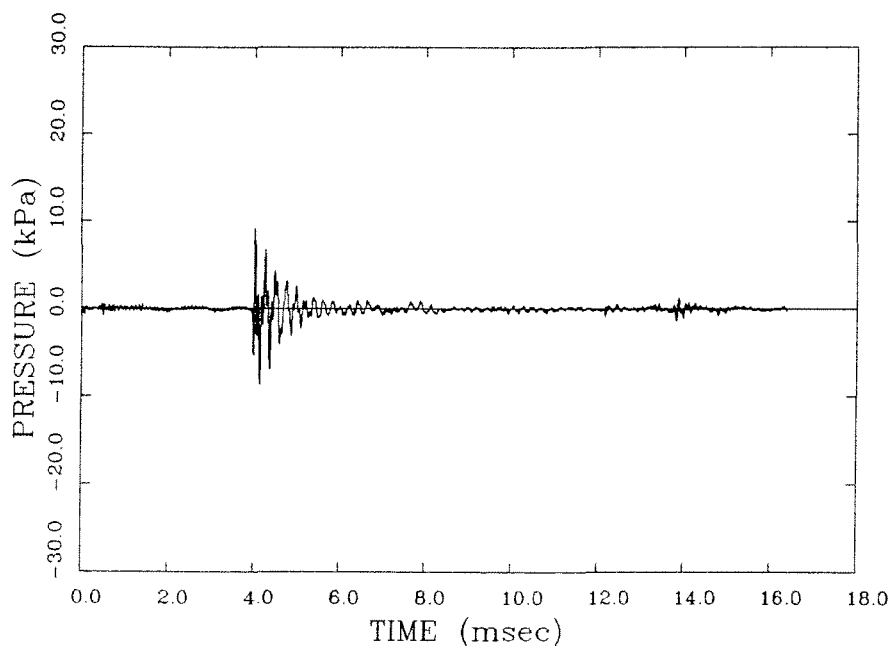


Figure 3.6.a. Bubble splitting waveform, $U_j=2.7$ m/s.

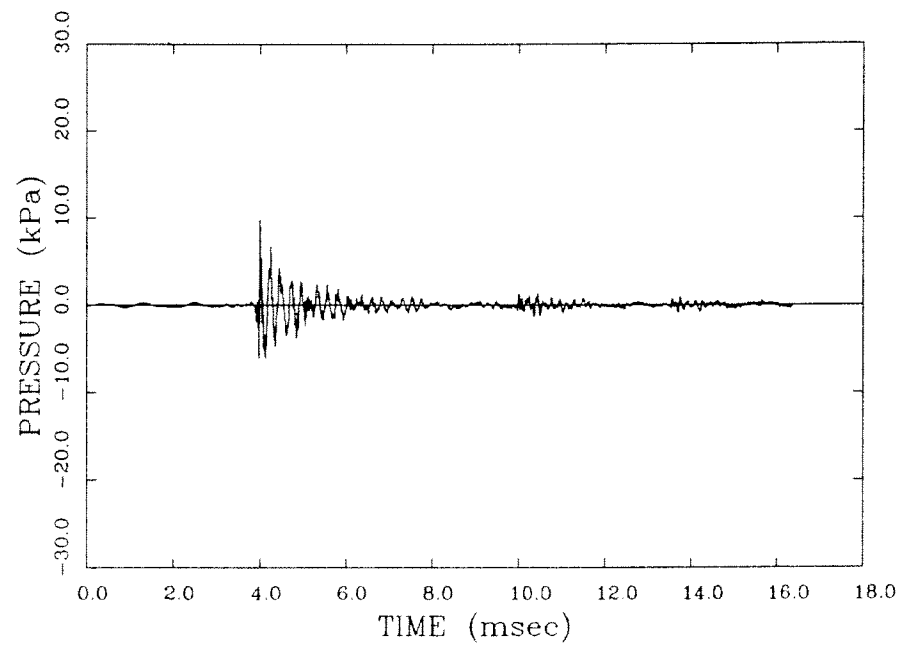


Figure 3.6.b. Bubble splitting waveform, $U_j = 5.0$ m/s.

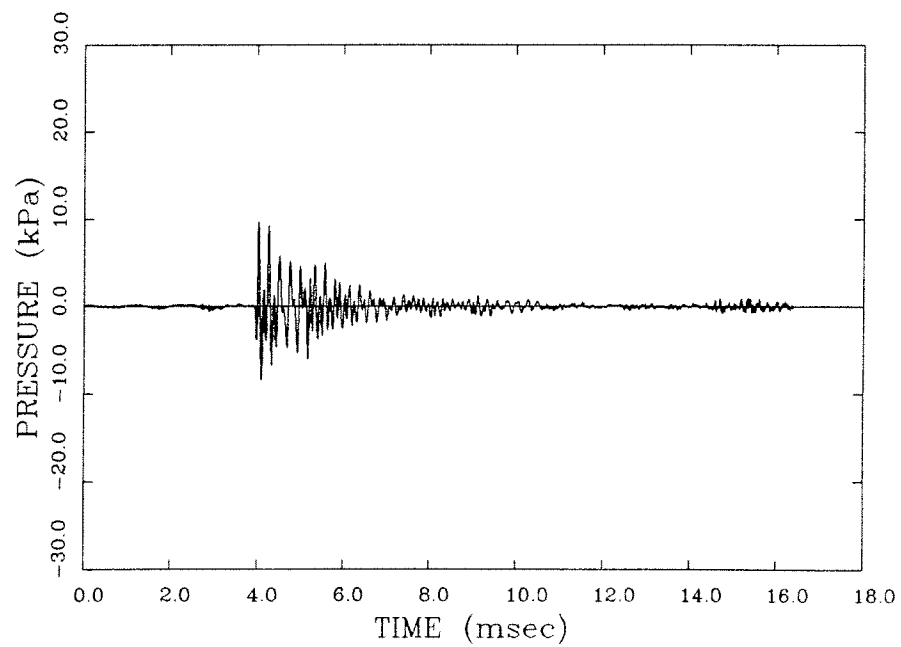


Figure 3.6.c. Bubble splitting waveform, $U_j = 7.5$ m/s.

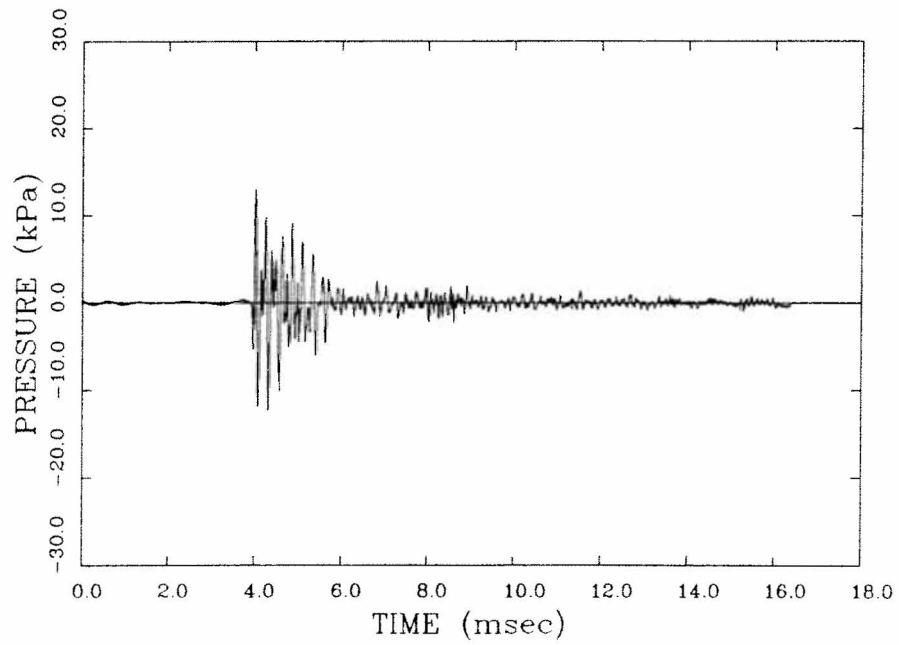


Figure 3.6.d. Bubble splitting waveform, $U_j = 10.0$ m/s.

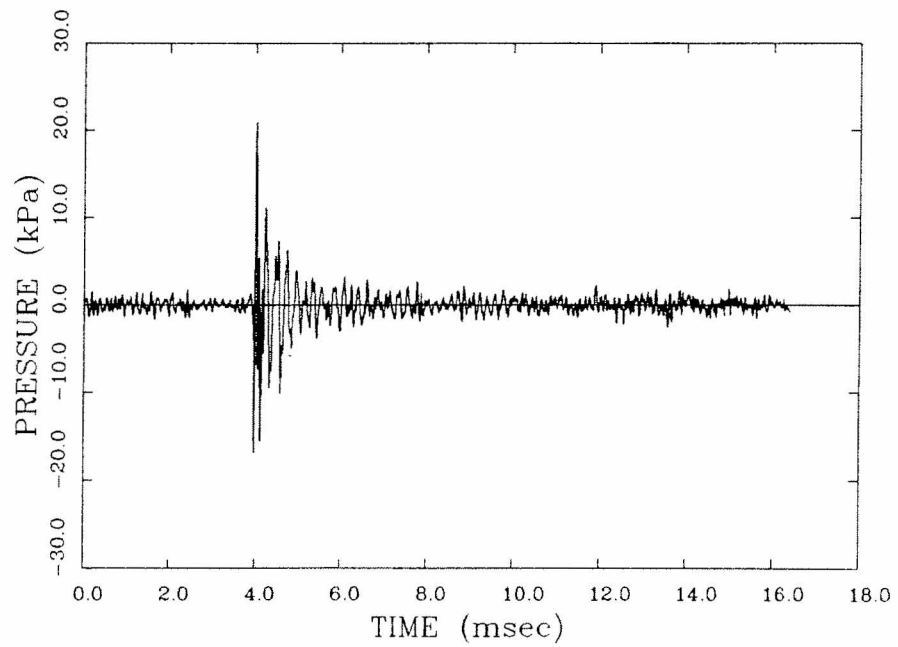


Figure 3.6.e. Bubble splitting waveform, $U_j = 12.5$ m/s.

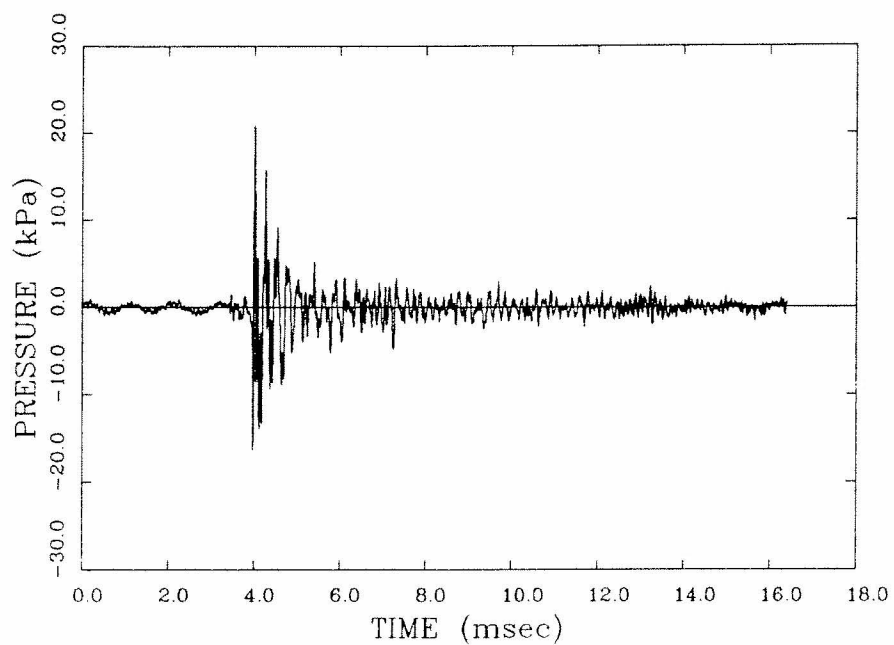


Figure 3.6.f. Bubble splitting waveform, $U_j=15.0$ m/s.

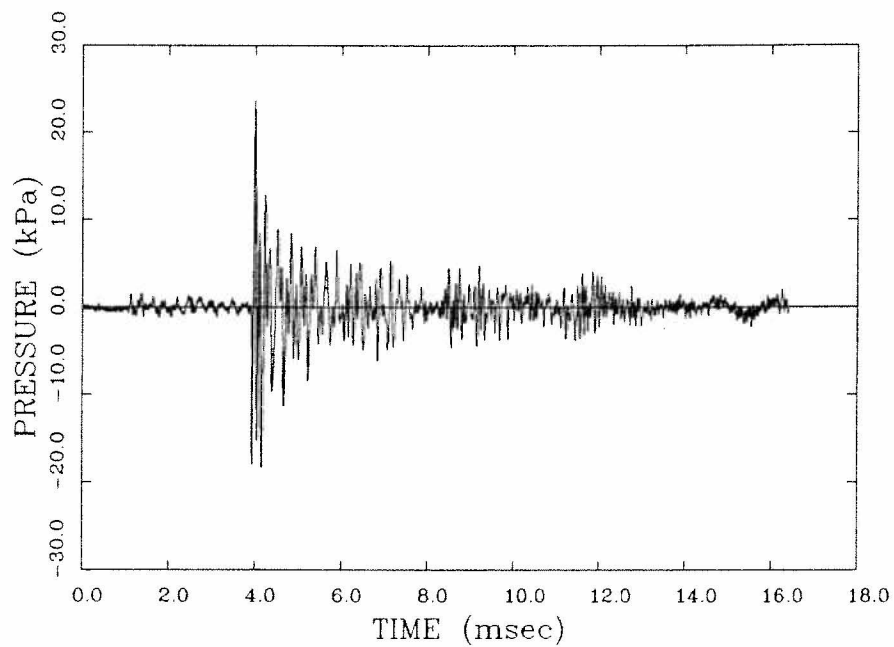


Figure 3.6.g. Bubble splitting waveform, $U_j=17.5$ m/s.

These results can be compared to a similar analysis of the background noise level at each jet velocity, i.e. no bubbles were being injected. The ambient sound levels were too high to adequately separate out the single-phase jet noise in the background measurements, figure 3.7.b. However, a general increase in the power spectral density with jet velocity was observed for the splitting events (figure 3.7.a), with a dramatic rise in the middle frequencies.

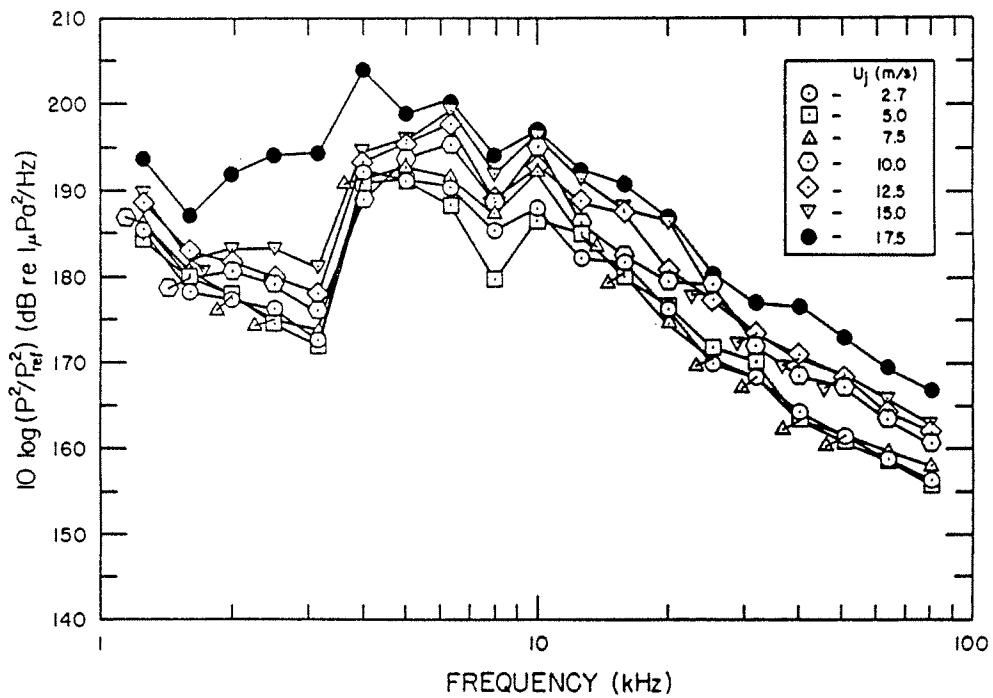


Figure 3.7.a One-third octave band analysis of averaged spectra from single splitting events.

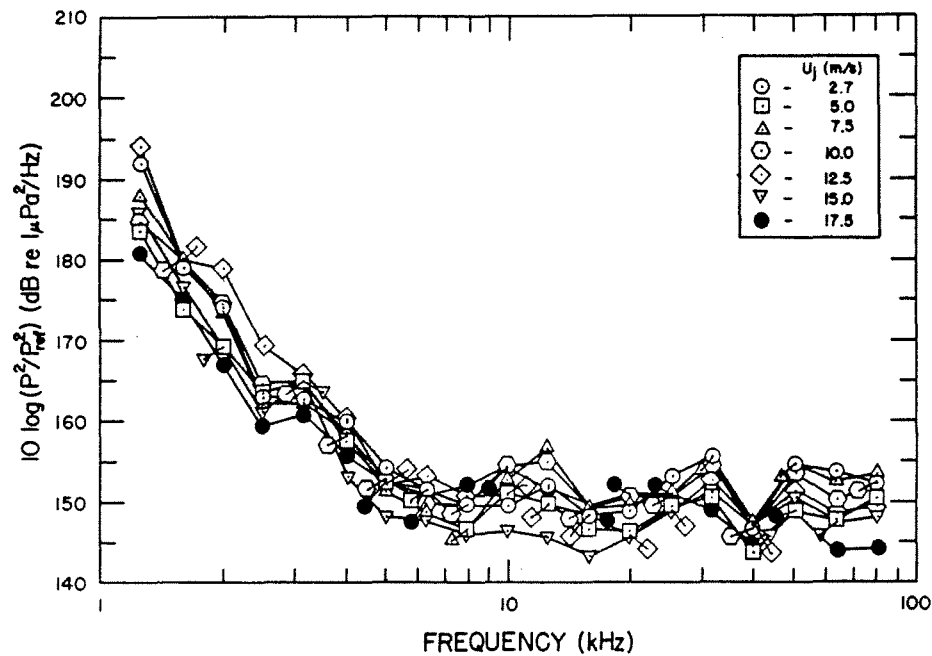


Figure 3.7.b One-third octave band analysis of background noise, no bubble injection.

3.4 DISCUSSION. The noise due to air bubbles splitting in turbulent shear layers has been a sparsely studied topic, with only a few analytical treatments and even fewer experiments. Several researchers have attempted to analyze splitting noise similarly to creation noise, i.e. by using equation 2.4 as the governing equation. This assumes the noise is due to the resulting oscillation of the bubble parts after they have split from the whole. The main difference from the creation noise problem is in the initial condition used to solve the differential equation. If it is assumed that the bubbles are deformed and split due to the interaction with the turbulent flow, the excess pressure P_+ , takes the form,

$$P_+ \approx R_0 \frac{\partial P}{\partial x_i} \quad (3.8)$$

where x_i is the direction the bubble will stretch when exposed to the local pressure gradient $\partial P/\partial x_i$. Photographs show that the bubbles do deform and stretch in the pressure field, figure 3.8. This leads to,

$$P_+ \approx \frac{R_0}{2} \rho_0 U_\infty^2 \frac{\partial C_p}{\partial x_i} \quad (3.9)$$

where C_p is the pressure coefficient, and U_∞ is the free stream velocity. As Blake (1984) shows, this assumption gives a U^4 speed dependence reflected in the acoustic pressure intensity. The only previous experimental evidence is found in Blake (1976), where his data show roughly a U^3 dependency on the power spectral density of the air emission noise in the wake of a hydrofoil. If the data collected in this thesis were analyzed in a similar manner, various results are obtained depending on the frequency band of interest. A U^3 to U^4 dependence is seen in the 20000- and 40000-Hz frequency band, however, the lower frequencies and the instantaneous peak values exhibit a U^2 behavior

Figure 3.8. Deformation of bubbles in the pressure gradient of the submerged jet.

Since no other experimental data exists to perform similar analysis, it is difficult to conclude which noise generating mechanism is dominant. In the present experiments, a feature which also affects the velocity dependence is the transition between near-field and far-field acoustic theory within the frequency range of interest. Depending on the frequency of the emitted noise, the frequency spectrum includes regions where the more complex near-field acoustic theory applies.

The bubble splitting mechanism and how it relates to noise generation is also of interest. Other researchers have shown that drop and bubble breakup largely results from an instability at the interface between the gas (or vapor) and the liquid, caused by locally unbalanced forces. Photographic evidence of splitting indicates that the process is violent, yielding numerous fragments of bubbles, figure 3.9.

Figure 3.9. Bubble splitting in the shear layer of the jet, jet velocity, $U_j = 7.5$ m/s.

This suggests that an instability is the driving force behind the splitting. The initial portion of the pressure waveforms for each velocity tested were reviewed. The waveform, triggered by the splitting, shows a time scale which is not strongly dependant on the jet velocity. This suggests that the turbulent flow may deform and excite the bubbles into oscillation, however, the splitting actually results from an instability. A closer look at the time scales reveals that for splitting, the first period of oscillation is approximately 100 μ s. A time scale characteristic of the turbulent flow field,

$$t_s = l/u', \quad (3.10)$$

where l is the characteristic eddy length and $u'=0.16U_j$ is the velocity fluctuation assuming Taylor's hypothesis, yields between 35 ms and 1700 ms for the range of velocities tested. The difference between the splitting time scale and the turbulent time scale translates into several orders of magnitude, leading one to believe that the noise resulting from bubble splitting will be more closely related to an instability rather than a motion driven by turbulent fluctuations. This hypothesis may also explain why the noise does not follow the predicted U^4 dependance.

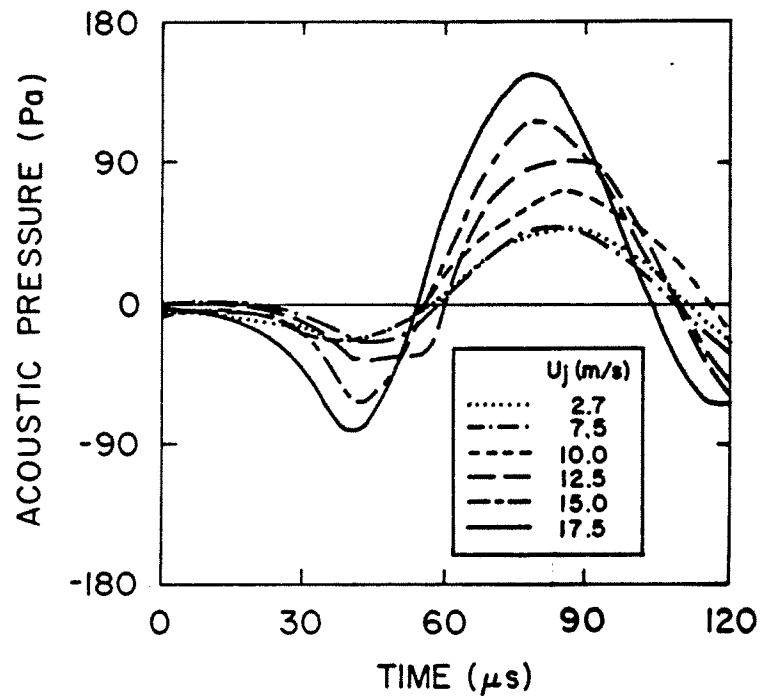


Figure 3.10. Initial period of bubble splitting noise waveform as a function of jet velocity.

CHAPTER 4

CONCLUSIONS AND RECOMMENDATIONS

4.1 SUMMARY OF THIS INVESTIGATION. Noise generation by the creation and splitting of air bubbles in water was found to be a substantial noise self producer. The formation, breakoff, and resulting oscillation of an air bubble from a nozzle submerged in quiescent water followed the basic theories developed by previous investigators quite closely.

The bubble oscillated in the zero mode or volumetric pulsation, at a frequency related to its diameter. Although higher order modes (fixed volume) were observed, no appreciable sound energy was radiated at frequencies related to those modes. The waveform of the oscillation was a classic damped (exponentially decaying) sinusoidal oscillation. This type of oscillation is characteristic of a damped free vibration. The damping is due to a combination of thermal, acoustic radiation, and viscous effects. The peak sound pressure generated by the bubble formation was predicted closely by the Rayleigh-Plesset equation, assuming the appropriate initial conditions are applied in the solution of the equation. The standard expressions for the initial conditions, did not properly predict the measured sound pressure levels. These expressions, derived from classical hydrodynamic theory, fall short of truly representing the actual physical processes occurring during the bubble formation and breakoff. A new model was developed which more closely

predicts the measured sound pressures. This model is based on an energy concept, in which the kinetic energy in the resulting bubble oscillation is equated to the work performed in the formation and breakoff of the bubble from a nozzle. The values of initial bubble wall velocity are of the same order as the values that were measured by Strasberg.

Bubbles splitting in a turbulent jet, was found to be a complex phenomenon. The mechanics of the bubble splitting along with the interaction of the dispersed phase with the turbulent structure of the continuous phase lead to some interesting problems. The experiments did lend some insight into the bubble splitting mechanism. The interaction with the turbulent structure of the mean flow caused substantial deformation of the bubbles. The excitation of the bubble into one or a combination of its vibrational modes lead to the development of an instability and the eventual breakup of the bubble. The time scale of a splitting event did not depend strongly on velocity. The acoustic pressures generated by the bubble breakup did exhibit some velocity dependence, although not the U^4 suggested by the available theory. Based on the frequency band of interest, anywhere from a direct proportionality to a fourth power dependence with velocity was observed in the power spectral density. Some effects of the test facility are noticed in this data, most notable was the transition between application of near-field and far-field acoustic theory within the frequency range of interest.

Analysis of the data based on an energy approach yielded an

anomaly. One could postulate that the noise generated by the bubble breakup is the difference in the energy of the bubble before and after the splitting. A surface energy analysis yields that the energy level in a cloud of bubbles resulting from the splitting of a single bubble is actually higher than that of the single bubble. This might indicate that energy is exchanged with the mean flow turbulence. Similar results have been found in cavitation research, Latorre (1987).

4.2 AREAS FOR FURTHER STUDY. Throughout the course of this study, several areas of interest were identified, where additional work could be done. In the area of bubble creation noise, the main interest for additional study would be on the effects of surface tension on the generation of acoustic pressures. A quite remarkable decrease (10 dB) was observed when the nozzle exterior was coated with a light oil prior to bubble generation. This implies that if the nozzle was made from a different material, such as teflon, that differences in the acoustic pressures generated by bubble creation might be realized. The solid-liquid-gas interface present in this application leads to a very difficult problem to solve theoretically and also quite difficult to control experimentally. Further research may have quite varied applications in process industries where noise from bubbling gas through a liquid is a problem.

The area of bubble splitting presents many more ideas for future work. One of the more interesting areas of study is the apparent instability driven breakup. Some evidence of this was found in the

present work, however much more research would be needed to show this conclusively. In a series of high-speed holograms by Hentschel and Lauterborn (1986), figure 4.1, a single bubble excited by acoustic waves into oscillation develops an instability and finally splits apart. While this example is not in a turbulent shear flow, the actual bubble splitting mechanism is probably very similar. As with Hentschel and Lauterborn's investigation, most prior work on drop and bubble deformation has been done under very controlled conditions, and not with turbulent flow conditions. Further study is needed to fully understand the interaction of the dispersed phase with the turbulent field. With increased understanding in this area, perhaps further insight into splitting mechanics and noise generation could be gained. Finally, many similarities between non-cavitating air-water flows and cavitating flows have been observed. Attempting to correlate information learned from the extensive studies of cavitating flows may lead to a faster and clearer understanding of the much less studied non-cavitating gas-liquid flows.

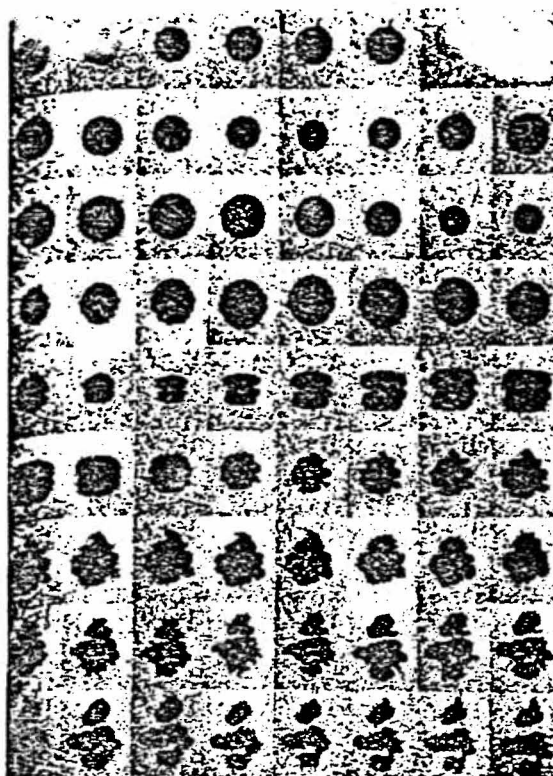


Figure 4.1. Excitation of an air bubble in quiescent water by acoustic radiation. (from Hentschel and Lauterborn).

REFERENCES

- Batchelor, G.K.**, "Pressure Fluctuations in Isotropic Turbulence," Proc. Cambridge Philisophical Society, Vol. 47, pt. 2, 1951, pp. 359-374.
- Batchelor, G.K.**, The Theory of Homogeneous Turbulence, Cambridge University Press, 2nd Edition, 1970.
- Bentley, B.J. and Leal, L.G.**, "An experimental investigation of drop deformation and breakup in steady, two-dimensional linear flows," Journal of Fluid Mechanics, Vol. 167, 1986, pp. 241-283.
- Blake, W. K.**, "Noise Generated by Single-orifice Air Emission from Hydrofoils," DTNSRDC Evaluation Report SAD-148E-1942, Aug. 1976.
- Blake, W.K.**, "Aero-Hydroacoustics for Ships," ITS DTNSRDC - 84/010, June 1984.
- Crighton, D. G. and Ffowcs-Williams, J. E.**, "Sound Generation by Turbulent Two-Phase Flow," Journal of Fluid Mechanics, Vol. 36, No. 3, 1969, pp. 585-603.
- Collins, S. B. and Knudsen, J. G.**, "Drop-Size Distributions Produced by Turbulent Pipe Flow of Immiscible Liquids," A.I.Ch.E. Journal, Nov. 1970, Vol. 16, No. 6, pp. 1072-1080.
- Devin, C., Jr.**, "Survey of Thermal, Radiation and Viscous Damping of Pulsating Air Bubbles in Water," Journal of the Acoustical Society of America, Vol. 31, No. 12, Dec. 1959, pp. 1654-1677.
- Franklin, R.E.**, "Jet Cavitation," Jets and Cavities - International Symposium, ASME Winter Annual Meeting, Miami, FL, Nov. 17-22 1985.
- Franklin, R.E., and McMillan, J.**, "Noise generation in cavitating flows, The submerged jet," ASME Journal of Fluids Engineering, Vol. 106, 1984, pp. 336-341.
- Gavigan, J. J., Watson, E. E. and King, W. F.**, "Noise Generation by Gas Jets in a Turbulent Wake," J. Acoust. Soc. Am., Vol. 56, 1974, pp.1094-1099.
- Han, C.D., and Funatsu, K.**, "An Experimental Study of Droplet Deformation and Breakup in Pressure-Driven Flows through Converging and Uniform Channels," Journal of Rheology, Vol. 22, No. 2, 1978, pp. 113-133.
- Hentschel, W., and Lauterborn, W.**, "High speed holographic movie camera," Optical Engineering, Vol 24, No. 4, July/August 1985, pp. 687-691

- Hinze, J. O., "Fundamentals of the Hydrodynamic Mechanism of Splitting in Dispersion Processes," A.I.Ch.E. Journal, Sept. 1955, Vol. 1, No. 3, pp. 289-295.
- Jorgensen, D. W., "Measurements of Noise from Cavitating Submerged Water Jets," David Taylor Model Basin Report 1126, Nov. 1958.
- Killen, J. M., "Bubble Noise Spectra in a Turbulent Boundary Layer," Symposium on Cavitation Noise, ASME Winter Meeting 1982, Phoenix, AZ, pp. 11-16.
- Lamb, H., Hydrodynamics, Dover Publications, New York, 1945, Sec. 294
- Latorre, R., "On the Discrepancy between Harrison's Estimate and Recent Observations of the Ratio of Cavitation Noise Energy to Initial Bubble Energy," Cavitation and Multiphase Flow Forum, ASME Applied Mechanics, Bioengineering, and Fluids Engineering Conference, Cincinnati, OH, June 14-17, 1987.
- Loehrke, R.I. and Nagib, H.M., "Control of Free-Stream Turbulence by Means of Honeycombs: A Balance Between Suppression and Generation," ASME Journal of Fluid Engineering, Vol. 98, No. 3, Sept. 1976, pp. 342-353
- Lumley, J.L. and McMahon, J.F., "Reducing Water Tunnel Turbulence by Means of a Honeycomb," ASME Journal of Basic Engineering, Vol. 89, Dec. 1967, pp. 764-770.
- Meyer, E. and Skudrzyk, E., Akust. Beih., Vol. 3, 1953, pp.434.
- Milne-Thompson, L.M., Theoretical Hydrodynamics, 4th Edition, The MacMillan Co., New York, 1960.
- Minnaert, M., "Musical Air Bubbles and the Sounds of Running Water," Philosophical Magazine, Vol. 16, 1933, pp. 235-248.
- Ooi, K.K., "Scale Effects on Cavitation Inception in Submerged Jets," CIT Engineering Report, 183-6, Dec. 1981
- Ooi, K. K. and Acosta, A. J., "The Utilization of Specially Tailored Air Bubbles as Static Pressure Sensors in a Jet," ASME Journal of Fluids Engineering, Vol. 106, Dec. 1984, pp. 459-465.
- Scheiman, J., "Comparison of Experimental and Theoretical Turbulence Reduction Characteristics for Screens, Honeycomb, and Honeycomb-Screen Combinations," NASA Technical Paper 1958, Science and Technical Information Branch, 1981.

- Sevik, M. and Park, S. H., "The Splitting of Drops and Bubbles by Turbulent Flow," ASME Journal of Fluids Engineering, Sept. 1973, pp. 53-60.
- Silberman, E., "Production of Bubbles by the Disintegration of Gas Jets in Liquids," Fifth Midwestern Conference on Fluid Mechanics, University of Michigan, 1957.
- Stinebring, D.R., "Scaling of Cavitation Damage," M.S. Thesis, The Pennsylvania State University, August 1976.
- Strasberg, M., "Gas Bubbles as Sources of Sound in Liquids," Journal of the Acoustical Society of America, Vol. 28, No. 1, Jan. 1956, pp. 20-26.
- Strasberg, M., "The Pulsation Frequency of Nonspherical Gas Bubbles in Liquids," Journal of the Acoustical Society of America, Vol. 31, No. 12, Dec. 1959, pp. 536-537.
- Taghavi, R., "Cavitation Inception in Axisymmetric Turbulent Jets," Ph.D. Thesis, University of Minnesota, Minneapolis, MN, 1985.
- Whitfield, O.J., and Howe, M.S., "The generation of sound by two-phase nozzle flows and its relevance to excess noise of jet engines," Journal of Fluid Mechanics, Vol. 75, part 3, 1976, pp. 553-576.

APPENDIX 1

Design of a Screened Diffuser

Large expansion ratio diffusers (half angle $> 3^\circ$), can experience separation, causing highly skewed and turbulent exit conditions. To avoid excessively long diffusers, screens may be placed within the wide angle diffuser in such a way as to prevent separation. The angle of a wide angled screened diffuser is usually selected between 30° and 90° . Angles less than 30° result in the pressure recovery coefficient increasing rapidly, while for angles greater than 90° , the distance between screens becomes impractically small. The choice of the screen mesh is generally a balance between losses through the screen and percent open area. In general, the rule of thumb is that open areas of 60 percent or greater should be maintained.

Our design requires an increase from 50.8 mm to 152.4 mm in diameter. A 32-mesh screen was chosen from standard available sizes. It has a 0.178 mm wire diameter and an open area of 60.59 percent. An angle of 45° was chosen for this diffuser design. Two options were evaluated; (1) a wide angle screened diffuser using 6 screens, and (2) a combination small angle/wide angle screened diffuser with 3 screens. The design procedure is as follows:

$$D_n = 0.1525 \text{ m (given)}$$

$$V_n = \left(\frac{D_o}{D_n}\right)^2 V_o = \left(\frac{0.051}{.1525}\right)^2 \times 7.5 = 0.839 \text{ m/s}$$

$$R_p = \frac{V_n d}{\rho \nu} = \frac{0.839 \times 0.178 \times 10^{-3}}{0.605 \times 10^{-6}} = 246$$

$$K = \frac{6.5(1-p)}{p^2} R_p^{-1/3} = 7.0145 R_p^{-1/3} = 1.12$$

$$C_p = 0.45 \quad (\text{from Miller})$$

where: D_* - diameter of the * section
 V_* - velocity in the * section
 R_p - equivalent Reynolds number
 d^p - screen wire diameter
 p - fraction of open area
 ν - kinematic viscosity
 K - pressure loss coefficient
 C_p - pressure recovery coefficient
 η_o^p - efficiency

Now the process repeats with the calculation of the first screen diameter,

$$D_{n-1} = \left(\frac{C_p \eta_o}{K} \right)^{1/4} D_n = \left(\frac{0.45 \times 1.05}{1.12} \right)^{1/4} 0.1525 = 0.123 \text{ m}$$

$$V_{n-1} = \left(\frac{D_o}{D_{n-1}} \right)^2 V_o = \left(\frac{0.051}{0.123} \right)^2 \times 7.5 = 1.29 \text{ m/s}$$

$$R_p = \frac{V_{n-1} d}{\rho \nu} = 294 \quad V_{n-1} = 379$$

$$K = \frac{6.5(1-p)}{p^2} R_p^{-1/3} = 7.0145 R_p^{-1/3} = 0.97$$

$$C_p = 0.43 \quad (\text{from Miller})$$

When the screen diameter matches the diameter of the given inlet, the calculations are stopped. If the design results in too many screens or if they are spaced too closely, modify the angle of the diffuser. It is mostly a matter of limitations in the available length that there is to work with. A summary of the design calculations is given in Table

A1.1. Final designs of the two schemes is in figure A1.1.

TABLE A1.1 - Design calculation for wide angled screened diffusers.

ITEM	VALUE	UNITS
diameter of outlet	0.1525	m
velocity of outlet	0.839	m/s
equivalent Reynolds No.	246	
pressure drop on screen	1.12	
pressure recovery in section	0.45	
diameter of screen	0.123	m
velocity in section	1.29	m/s
equivalent Reynolds No.	379	
pressure drop on screen	0.97	
pressure recovery in section	0.43	
diameter of screen	0.101	m
velocity of section	1.91	m/s
equivalent Reynolds No.	562	
pressure drop on screen	0.85	
pressure recovery in section	0.4	
diameter of screen	0.085	m
velocity of section	2.7	m/s
equivalent Reynolds No.	794	
pressure drop on screen	0.76	
pressure recovery in section	0.38	
diameter of screen	0.072	m
velocity of section	3.76	m/s
equivalent Reynolds No.	1106	
pressure drop on screen	0.678	
pressure recovery in section	0.36	
diameter of screen	0.062	m
velocity of section	5.04	m/s
equivalent Reynolds No.	1483	
pressure drop on screen	0.615	
pressure recovery in section	0.35	

$$\text{diameter of inlet: } D_{n-6} = \left(\frac{C_p \eta_0}{K} \right)^{\frac{1}{4}} D_{n-5} = 0.054 \text{ m.}$$

This is very close to the given inlet diameter of 0.051 m. The combination small/wide angle diffuser simply uses the same calculations, but terminates the wide angle section at such a location as to allow for a small angle diffuser to be used. This combination is mostly dependent on any length constraints present. In this case, the wide angle diffuser was terminated at the third screen leaving a 0.38 m long, 2.56° half angled section to complete the reduction.

REFERENCE

Miller, D.S., *INTERNAL FLOW: A guide to losses in pipe and duct systems*, BHRA, 1971.

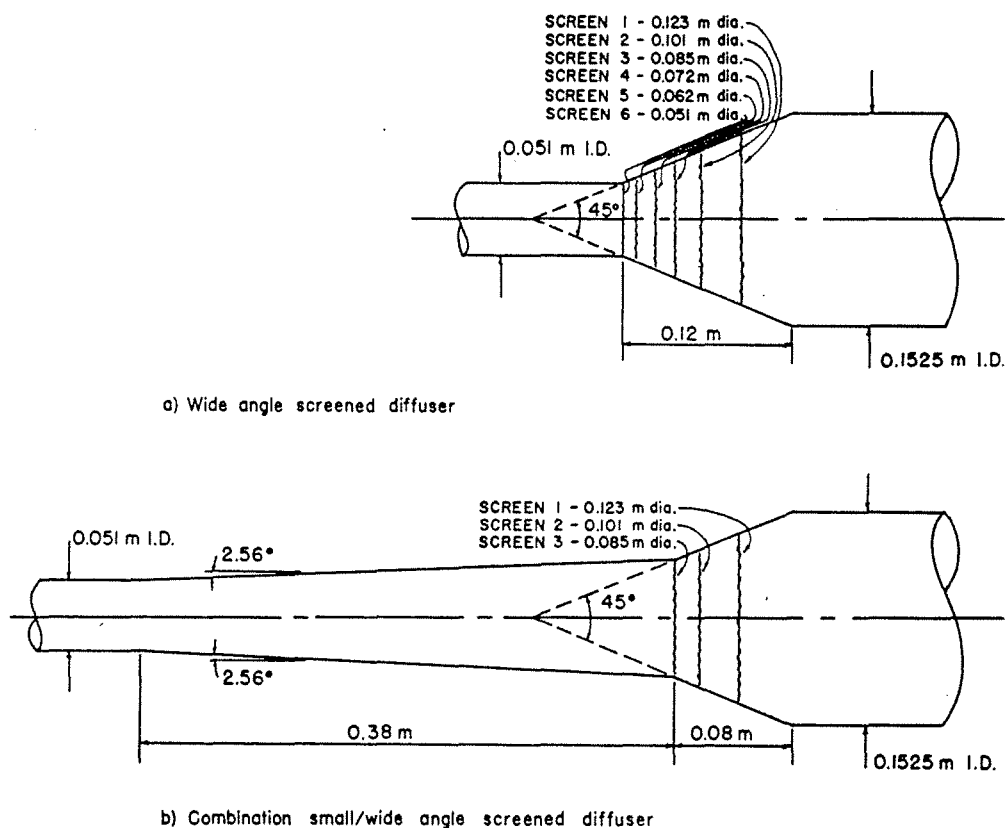


Figure A1.1. Final design for a wide-angle screened diffuser.